Fractal Magnetic Microstructure in the $(Co_{41}Fe_{39}B_{20})_x(SiO_2)_{1-x}$ Nanocomposite Films

R. S. Iskhakov[a,*], S. V. Komogortsev[a], E. A. Denisova[a], Yu. E. Kalinin[b], and A. V. Sitnikov[b]

*[a] Kirensky Institute of Physics, Siberian Branch, Russian Academy of Sciences,
Akademgorodok, Krasnoyarsk, 660036 Russia
e-mail: rauf@iph.krasn.ru
[b] Voronezh State Technical University, Moskovskiĭ pr. 14, Voronezh, 394026 Russia

Received August 8, 2007

Magnetostructural methods are applied to determine the exchange bond percolation limit in $(Co_{41}Fe_{39}B_{20})_x(SiO_2)_{1-x}$ nanocomposites ($x_c \approx 0.30 \pm 0.02$), which separates the phase plane along the metal concentration axis into a superparamagnetic region and a ferromagnetic region. It is shown that, with respect to the singularities of the magnetization up to the magnetization saturation curves, the ferromagnetic region is further subdivided into three regions differing in the character of the spatial propagation of the magnetization ripples or in the magnetic correlation function characteristics. The fractal dimension of the nanocomposite magnetic microstructure near the percolation threshold is determined.

PACS numbers: 75.30.Gw, 75.50.Kj, 75.60.-d

1. Magnetic nanostructures (either natural or artificial) consist of magnetic nanoparticles (~10 nm in size) and are characterized by different geometries of the spatial arrangement of these particles, which forms either low-dimensional spin systems (nanofilaments, multilayers) or intricate bulk structures. Under strong exchange interaction between the nanoparticles, the relation between the macroscopic magnetic parameters of the nanomagnetic (such as the susceptibility, coercive field, and residual magnetization) and the microscopic parameters of the spin system (such as the nanoparticle (grain) size, inter- and intragrain exchange interaction, and local anisotropy) is described by the so-called random anisotropy model [1–4] proposed for amorphous ferromagnetic materials.

Random anisotropy results in the destruction of the ferromagnetic long-range order in the spin system; however, owing to the exchange interaction, the ferromagnetic order is restored at the characteristic lengths R_L of the magnetic orientation coherence. The investigations revealed that the macroscopic magnetic characteristics of nanomagnets are determined by the dimension $2R_L$ and the anisotropy of stochastic domains spontaneously formed by a large number of particles ($2R_c$ in size).

At the Institute of Physics, Siberian Branch, Russian Academy of Sciences, a method has been theoretically and experimentally developed which makes it possible to determine, from the curves of magnetization up to the saturation magnetization in nanomagnets, the size

of their micromagnetic surface element (stochastic domain size), the magnitude of the effective anisotropy in this element, and the size of the nanostructure element (nanoparticle size) and its local anisotropy, as well as the spatial dimension of the system of exchange-coupled ferromagnetic nanoparticles (see, e.g., [5]). This method was tested on chains of exchange-coupled grains with random anisotropy (ferromagnetic metal nanofilaments in carbon nanotubes) [6] on ultrathin films formed by the two-dimensional packing of exchange-coupled grains [7, 8] as well as on amorphous and nanocrystalline ferromagnetic foils and coatings whose spin system is formed by the three-dimensional packing of exchange-coupled grains [7–9].

The objective of this paper is to investigate, using the above method, the (ferromagnetic metal–dielectric) nanocomposites by example of the $(Co_{41}Fe_{39}B_{20})_x(SiO_2)_{1-x}$ granulated alloy. Giant magnetoresistance, giant anomalous Hall effect, intensification of magneto-optical effects, and other interesting physical effects were revealed in these materials [10–12]. These effects are mainly due to the micromagnetic structure features of these materials. Our goal is to reveal these features. Since they are associated with the atomic microstructure of the nanocomposite under study, we provide some information on the microstructure of the granulated (ferromagnetic metal–dielectric) nanocomposites.

The microstructure of these nanocomposites is in many respects determined by the simplicity of the $3d$-metal nanograin formation in the SiO_2 (or Al_2O_3)
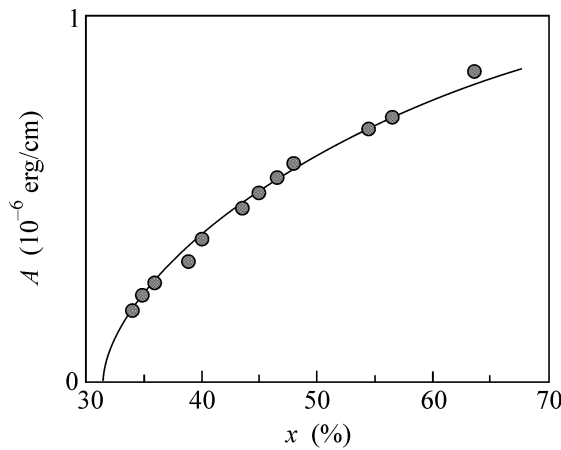
Fig. 1. Exchange coupling constant in $(Co_{41}Fe_{39}B_{20})_x(SiO_2)_{1-x}$ nanocomposite films. The solid line is the dependence $A(x) = A_0(x - x_c)^{0.5}/(1 - x_c)^{0.5}$, where $x_c = 0.32$ and A_0 is the exchange-interaction magnitude in the amorphous $Co_{41}Fe_{39}B_{20}$ alloy.

oxide dielectric matrix. Since the surface energy of the 3d metals is three or four times higher than that of the given oxides, metal grain morphology is close to spherical shape in the oxide matrix. Particularly, this grain shape is realized at a low metal phase concentration. Here, the nanograins are electrically insulated from one another, so that the conductivity of these composites is mainly determined by the oxide. The number of nanograins increases with the metal phase concentration and they start to form small conglomerates and chains, which, in turn, form a labyrinth-like microstructure. At a certain phase ratio (called the percolation threshold), the metal nanograins form a peculiar grid over which the metal conduction takes place. The numerical simulation predicts three morphological types of the two-phase mixture, depending on the volume fraction of the metal grains. At a metal volume fraction less than 0.3, isolated metal particles chaotically distributed over the dielectric matrix dominate. At a volume fraction from 0.3 to 0.7, both phases (metal and dielectric) form bound grids. At metal volume fractions above 0.7 (the second percolation threshold), phase microstructure inversion takes place: the metal grains form the conducting matrix, and the dielectric is represented by insulated particles.

Now, we demonstrate how the structural transformation of the nanocomposites affects their basic magnetic parameters and the actual micromagnetic structure.

2. The $(Co_{41}Fe_{39}B_{20})_x(SiO_2)_{1-x}$ nanocomposites were prepared by ion-beam sputtering of compound targets in argon on a unit specially designed at Voronezh State Technical University. The material was deposited on uncooled sitall substrates under conditions providing the deposited film purity and an extremely low Ar content in the samples (less than 0.1 at %). In the deposition process, the substrate temperature did not exceed 393 K, and the films obtained were 3–4 μm thick. The microstructure of the nanocomposites obtained was investigated by transmission electron microscopy, and their composition was controlled by electron-probe x-ray microanalysis [10]. The electric properties and magnetoresistance effect of the nanocomposites were measured by the two-probe potentiometer method. The magnetic properties were studied by a vibration magnetometer.

In these nanocomposites, the electric resistance dependence on the metal phase concentration in the range $0.3 < x < 0.7$ is S-shaped with a single inflection point near the percolation threshold. The threshold magnitude x_c is reliably determined at the point of intersection of the electric resistance concentration dependences for initial and heat-treated nanocomposites. Thermal annealing leads to an increase in the nanocomposite electric resistance with the metal phase concentration $x < x_c$ and to its decrease for nanocomposites with $x > x_c$. The x_c value was additionally determined by the point of the maximum of the magnetoresistance dependence on the metal phase concentration. The x_c value thus determined was about 0.5 for the $(Co_{41}Fe_{39}B_{20})_x(SiO_2)_{1-x}$ nanocomposites.

The field and low-temperature dependences of magnetization, $M(T, H)$, for the given nanocomposites were measured in an external field range up to 12 kOe and at 90–300 K. The external field was directed parallel to the film surface.

3. The temperature dependence of the saturation magnetization in the films was measured at $H = 12$ kOe. In the concentration range chosen ($0.3 < x \leq 0.7$), the curves $M(T)$ for all the nanocomposites were characterized by negative curvature and were well described by the Bloch law, $\Delta M(T)/M_s = BT^{3/2}$, at B varying from 6×10^{-6} K$^{-3/2}$ to 23×10^{-6} K$^{-3/2}$. With the use of the standard expressions [13] and the constant B, the exchange interaction constant A was calculated. Figure 1 presents the A values obtained for the nanocomposites studied.

The magnetization curves were measured in fields up to 12 kOe and plotted in log–log coordinates [$(M_s - M)/M_s$, H], allowing us to reveal the power dependences $\Delta M \sim H^{-\alpha}$ and to determine the exponents and tangents of these dependences. The $(Co_{41}Fe_{39}B_{20})_x(SiO_2)_{1-x}$ nanocomposites may be subdivided into three types in the concentration range studied by peculiar features of the curves of magnetization up to the saturation magnetization. Figure 2 presents the magnetization curves characterizing each nanocomposite type. Since the shape of the $M(H)$ curve is determined by the magnetic microstructure, the characteristics of the magnetic correlation function (dispersion and magnetic correlation radius) of the first, second, and third types of nanocomposite differ considerably. Actually, for the first type of nanocomposite ($x > 0.6$) in strong fields, the dependence $\Delta M \sim H^{-2}$ is real-

ized, which transforms to $\Delta M \sim H^{-1/2}$ as the field decreases (see the inset in Fig. 2). For the second type of nanocomposite ($0.39 \leq x \leq 0.6$), the dependence $\Delta M \sim H^{-2}$ first transforms to $\Delta M \sim H^{-1}$ as the field decreases and only then to $\Delta M \sim H^{-1/2}$ (see Fig. 2). Finally, for the third type of nanocomposite ($0.3 < x \leq 0.38$), the dependence $\Delta M \sim H^{-2}$ transforms to $\Delta M \sim H^{-\alpha}$ with α varying from 1.05 to 1.4. The measurements of the exponent α as a function of the metal phase concentration and the external field are presented in Fig. 3.

4. Now we discuss the experimental results obtained and presented in Figs. 1–3. We begin with the exchange interaction concentration dependence $A(x)$ (see Fig. 1). The experimental points fit well the root parabola $A(x) = A_0(x - x_c)^{0.5}(1 - x_c)^{-0.5}$, where the coefficient A_0 is the exchange interaction magnitude of the $Co_{41}Fe_{39}B_{20}$ amorphous alloy [14] and $x_c = 0.32$ points to the percolation threshold with respect to the interparticle exchange bonds. The point (x_c) separates the phase plane along the metal concentration axis into a superparamagnetic region (interparticle exchange is absent) and a ferromagnetic region, where the interparticle exchange magnitude is a nonlinear function of x_c and asymptotically approaches the intraparticle exchange magnitude A_0 (as $x \longrightarrow 1$). We note that the x_c value is close to the first percolation threshold obtained by numerical simulation and differs considerably from $x_c \approx 0.5$ obtained from the experimental dependences of the electric resistance and magnetoresistance.

Then, we analyze the magnetization curves $M(H)$. In the range of strong fields (where magnetization approaches saturation) at all x values of the $(Co_{41}Fe_{39}B_{20})_x(SiO_2)_{1-x}$ nanocomposites investigated, these curves agree well with the well-known Akulov law (see Fig. 2)

$$M = M_s\left(1 - \left(\frac{aH_a}{H}\right)^2\right). \quad (1)$$

Here, $H_a = 2K/M_s$ is the local magnetic anisotropy field and a is the numerical symmetry coefficient equal to $1/15^{1/2}$ for uniaxial anisotropy. This allowed us to calculate the rms fluctuation of the local magnetic anisotropy field aH_a (see Fig. 4). It is seen that aH_a for $x > 0.5$ is constant and is equal to its value in the amorphous (CoFeB) alloy bands measured in [14]. As the metal phase decreases for $x \leq 0.46$, the local magnetic anisotropy field increases exponentially. As the field decreases for $H < H_R = 2A/MR_c^2$, the $M(H)$ function changes its shape. The corresponding theory and calculated functional dependences are presented in [15, 16]. We call attention to the physical meaning of the changes recorded. They are attributed to the appearance and propagation of exchange-correlated magnetic deviations in the spin system (these deviations were called magnetization ripples in metal films). As shown in [17], the ripple length $R_H = (2A/MH)^{1/2}$ in the exchange-cor-
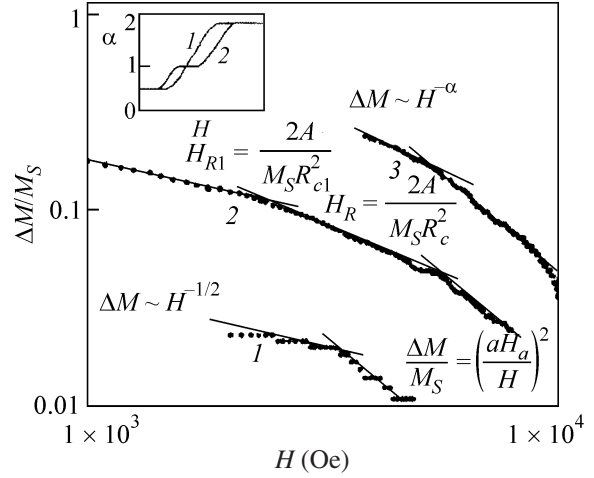

Fig. 2. Magnetization deviation from saturation in the $(Co_{41}Fe_{39}B_{20})_x(SiO_2)_{1-x}$ composite films with $x =$ (from top to bottom) 37, 42, and 68%.
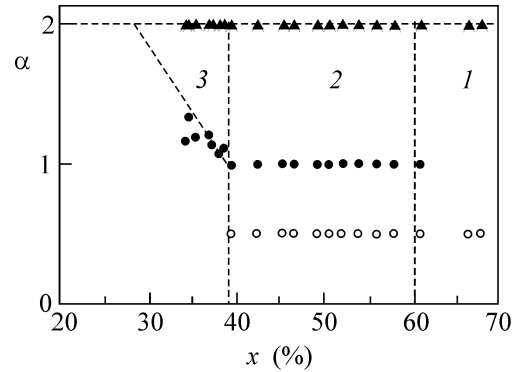

Fig. 3. Exponent α in the asymptotic dependences of magnetization up to the magnetization saturation $\Delta M \sim H^{-\alpha}$ in the $(Co_{41}Fe_{39}B_{20})_x(SiO_2)_{1-x}$ composite films.

related systems with random anisotropy is bounded from below and above: $R_c \leq R_H \leq R_L$. Therefore, the $M(H)$ function at $H_L = 2A/MR_L^2 < H < H_R = 2A/MR_c^2$ can be determined from Eq. (1), where the local anisotropy H_a of the particle is replaced by the effective anisotropy of the region covered by a single ripple length R_H,

$$\langle H_a \rangle_{R_H} = \frac{H_a}{\sqrt{N}} = H_a\left(\frac{R_c}{R_H}\right)^{d/2} = H_a\left(\frac{H}{H_R}\right)^{d/4}. \quad (2)$$

Then, instead of Eq. (1), we obtain

$$\frac{M_s - M}{M_s} = \frac{(aH_a)^2}{H_R^{d/2}}\frac{1}{H^{(4-d)/2}}$$

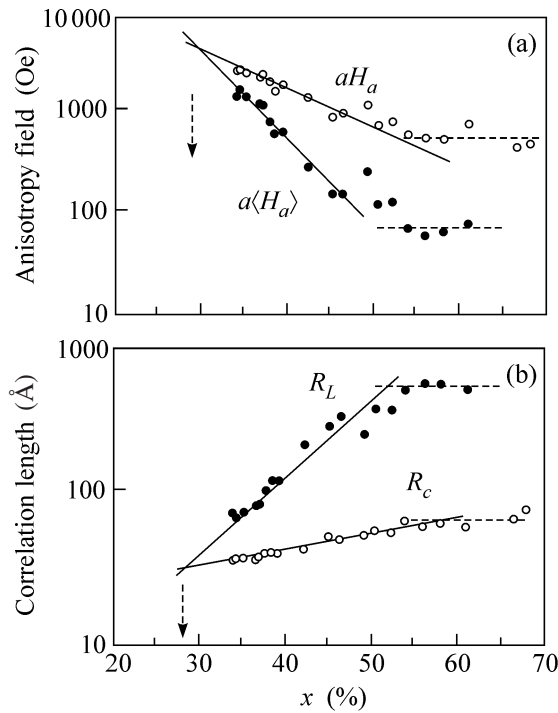$$= \frac{(a\langle H_a \rangle_L)^2}{H_L^{d/2}}\frac{1}{H^{(4-d)/2}}, \quad H_L < H < H_R. \quad (3)$$

Fig. 4. (a) Magnetic anisotropy field in the stochastic domain $a\langle H_a \rangle_L$ and the local magnetic anisotropy field aH_a in $(Co_{41}Fe_{39}B_{20})_x(SiO_2)_{1-x}$ composite films. (b) Stochastic magnetic domain size R_L and the structural correlation length R_c.

Here, d is the dimension of the ferromagnetic grain and $\langle H_a \rangle_L = 2\langle K \rangle_L / M_s$ is the macroscopic anisotropy field in a stochastic domain defined as

$$\langle H_a \rangle_L = H_a \left(\frac{H_L}{H_R} \right)^{d/4} = H_a \left(\frac{R_c}{R_L} \right)^{d/2} = \frac{H_a}{\sqrt{N}}, \quad (2')$$

where N is the number of nanoparticles in the stochastic domain.

The given approach makes it possible to relate the revealed subdivision of the nanocomposite ferromagnetic region with respect to concentration into three subregions (see Fig. 3) with the characteristic propagation of the magnetization ripples. For $x > 0.6$, the three-dimensional propagation of ripples is observed leading to the dependence $\Delta M \sim H^{-1/2}$; for $0.39 \leq x \leq 0.6$, the two-dimensional propagation of short-wavelength ripples ($\Delta M \sim H^{-1}$) and the three-dimensional propagation of long-wavelength ripples ($\Delta M \sim H^{-1/2}$) occur; for $0.33 \leq x \leq 0.38$, the fractal propagation of the magnetization ripples ($\Delta M \sim H^{-\alpha}$) proceeds. Since the concentration dependence $\alpha(x)$ is established in this region (see Fig. 3), the fractal dimension d can be calculated from Eq. (3). It varies from 1.2 to 1.9, depending on the metal concentration.

The character of the magnetization ripple propagation is determined by the configuration of the ferromagnetic grain spatial packing in the nanocomposites. Hence, the data obtained from the magnetization curves indicate the spatial grain packing in the first region, the plane morphology of the conglomerates of grains vertically chain-linked in the second region, and the fractal grain packing in the third region (see Fig. 3).

We note one more point. If the $\alpha(x)$ dependence in the third region in Fig. 3 is described by a linear function, then its extrapolation to the ordinate $\alpha = 2$ will also allow us to find the percolation threshold (the exchange-coupled particles obey expression (3), where $d = 0$, $H_L = H_R$, and $\langle H_a \rangle_L = H_a$). The critical concentration thus determined for the metal phase is $x_c = 0.28$. The R_c values were calculated from the experimental $H_R(x)$ values (see Fig. 4) and $a\langle H_a \rangle_L$ and R_L were calculated in the approximation $H_L \approx a\langle H_a \rangle_L$. It is seen that, for $x \leq 0.46$, R_L and R_c decrease exponentially, and $a\langle H_a \rangle_L$ increases exponentially (as H_a) as x decreases. The conditional extrapolation of these dependences (see Fig. 4) also estimates the threshold, $x_c = 0.28$. Therefore, from the curves $A(x)$ (Fig. 1), $\alpha(x)$ (Fig. 3), R_L, R_c, $\langle H_a \rangle_L$, and $H_a - f(x)$ (Fig. 4), we obtain the estimate $x_c = 0.30 \pm 0.02$ for the metal phase critical concentration in the $(Co_{41}Fe_{39}B_{20})_x(SiO_2)_{1-x}$ nanocomposite, at which the spin system can be represented as superparamagnetic.

To conclude, we note that the method of correlation magnetometry based on the analysis of curves of magnetization up to the magnetization saturation has been used in this study to determine the fractal dimension of the spatial configuration of magnetic grains in nanocomposites.

REFERENCES

1. R. Harris, M. Plischke, and M. J. Zukermann, Phys. Rev. Lett. **31**, 160 (1973).

2. V. A. Ignatchenko and R. S. Iskhakov, Zh. Éksp. Teor. Fiz. **72**, 1005 (1977) [Sov. Phys. JETP **45**, 526 (1977)] Izv. Akad. Nauk SSSR, Ser. Fiz. **44**, 1434 (1980).

3. R. Alben, J. J. Becker, and M. C. Chi, J. Appl. Phys. **49**, 1653 (1978).

4. E. M. Chudnovsky, W. M. Saslow, and R. A. Serota, Phys. Rev. B **33**, 251 (1986).

5. R. S. Iskhakov and S. V. Komogortsev, Izv. Ross. Akad. Nauk, Ser. Fiz. **71**, 1661 (2007).

6. R. S. Iskhakov, S. V. Komogortsev, A. D. Balaev, et al., Pis'ma Zh. Éksp. Teor. Fiz. **78**, 271 (2003) [JETP Lett. **78**, 236 (2003)].

7. R. S. Iskhakov, V. A. Ignatchenko, S. V. Komogortsev, et al., Pis'ma Zh. Éksp. Teor. Fiz. **78**, 1142 (2003) [JETP Lett. **78**, 646 (2003)].

8. R. S. Iskhakov, S. V. Komogortsev, A. D. Balaev, et al., Pis'ma Zh. Éksp. Teor. Fiz. **72**, 440 (2000) [JETP Lett. **72**, 304 (2000)].

9. R. S. Iskhakov, S. V. Komogortsev, Zh. M. Moroz, and E. E. Shalygina, Pis'ma Zh. Éksp. Teor. Fiz. **72**, 872 (2000) [JETP Lett. **72**, 603 (2000)].

10. O. V. Stogneĭ, Yu. E. Kalinin, A. V. Sitnikov, et al., Fiz. Met. Metalloved. **91** (1), 24 (2001) [Phys. Met. Metallogr. **91**, 21 (2001)].

11. Yu. E. Kalinin, A. V. Sitnikov, N. E. Skryabina, et al., Pis'ma Zh. Tekh. Fiz. **29** (9), 18 (2003) [Tech. Phys. Lett. **29**, 361 (2003)].

12. I. V. Zolotukhin, Yu. E. Kalinin, A. T. Ponomarenko, et al., J. Nanostruct. Polym. Nanocompos. **2**, 23 (2006).

13. R. S. Iskhakov, G. V. Popov, and M. M. Karpenko, Fiz. Met. Metalloved. **56**, 85 (1983).

14. R. S. Iskhakov, M. M. Karpenko, G. V. Popov, and V. P. Ovcharov, Fiz. Met. Metalloved. **61**, 265 (1986).

15. V. A. Ignatchenko, R. S. Iskhakov, and G. V. Popov, Zh. Éksp. Teor. Fiz. **82**, 1518 (1982) [Sov. Phys. JETP **55**, 878 (1982)].

16. V. A. Ignatchenko and R. S. Iskhakov, Fiz. Met. Metalloved., No. 6, 75 (1992) [Phys. Met. Metallogr. **73**, 602 (1992)].

17. S. V. Komogortsev and R. S. Iskhakov, Fiz. Tverd. Tela (St. Petersburg) **47**, 480 (2005) [Phys. Solid State **47**, 495 (2005)].

Translated by E. Perova